Water Environment Research

RESEARCH ARTICLE

Assessing *Acinetobacter junii* MKVVM4 IITBHU Mediated Remediation for As(III) and As(V)

Manoj Kumar Verma | Vishal Mishra

School of Biochemical Engineering, Indian Institute of Technology (BHU), Varanasi, Uttar Pradesh, India

Correspondence: Manoj Kumar Verma (manojkverma.rs.bce18@itbhu.ac.in)

Received: 9 March 2025 | **Revised:** 26 May 2025 | **Accepted:** 3 June 2025

Funding: This work is supported by the Indian Institute of Technology (BHU) Varanasi, India.

Keywords: *Acinetobacter junii* MKVVM4 IITBHU | arsenic | As(III) | As(V) | bioremediation | gene | resistant

ABSTRACT

In the present work, an arsenic (As) resistant bacterium has been isolated from the Ganga River, Varanasi, Uttar Pradesh, India. The isolate was identified as *Acinetobacter junii* MKVVM4 IITBHU (NCBI accession no. ON248394). *A. junii* MKVVM4 IITBHU could grow in As(V) and As(III) up to 4000 and 3000 ppm, respectively. The isolated strain showed amplification of genes like a*rs*C (As(V) reductase), *aio*A (As(III) Oxidase), *arr*A (As(V) respiratory reductase), and a*rs*M (As(III) S adenosylmethionine methyltransferase) in targeted amplification. SEM images of *A. junii* MKVVM4 IITBHU showed that bacterial cells in the initial development phase had coccobacilli-like morphology having a tail. Elemental mapping and EDS spectrum confirmed the arsenic accumulation within the bacterial cells. There were peak shifts of negatively charged functional groups like amine, alkenes, carboxyl, and hydroxyl in As(III) and As(V) mediums compared to the control group on the cell surface. This work gives insight into the resistance mechanism of *A. junii* MKVVM4 IITBHU against arsenic. The present work also reports the metabolic requirements of *A. junii* MKVVM4 IITBHU for environmental persistence and its potential utility in the bioremediation of As(III) and As(V) from the contaminated sites.

Summary

- The isolate can tolerate 4000 and 3000 ppm of As(V) and As(III), respectively.
- Bacterial arsenic-resistant gene amplification explains arsenic bioremediation.
- As(V) facilitated the rapid growth of the isolate as compared to the Control.
- The diauxic growth in the As(V) medium indicated towards the preferred substrate.
- Isolate in the early stage of growth showed a tailed structure.

1 | Introduction

The weathering of rocks, minerals, and other anthropogenic sources contaminate soil and groundwater. Biological transformation, pH of water, presence of competing ions, and arsenic (As) speciation affect the As concentration and mobility in the groundwater (Ghosh and Singh 2010). Poisoning in human beings causes disorders like skin lesions, respiratory and neurological disturbance, and malignancies of various forms. Humans are exposed to As through contaminated water, foods, cigarette smoking, occupational environments, and cosmetics (Chung et al. 2014).

As is a metalloid that has no flavor or odor. The two most prevalent valences of As present in the groundwater are oxidized arsenite (AsO^{2-} or As(III)) and arsenate ($AsO4^{-3}$or As(V)) (Luong et al. 2007). The toxicity of As(III) is 60 times more than that of As(V). In general, organic As is less hazardous than inorganic

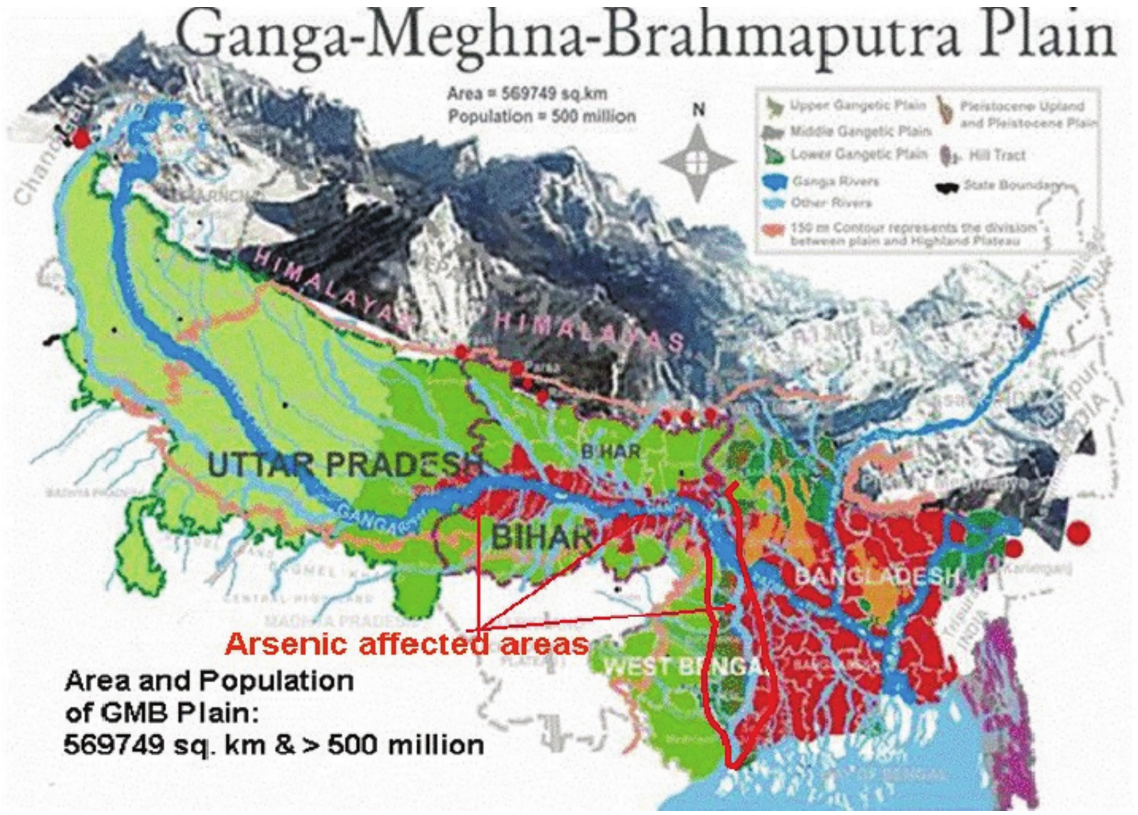

FIGURE 1 | As-affected areas of India. Figure adapted from Ghosh and Singh (2010) with permission.

one. It cannot be eliminated from the environment and can only be transformed into a less harmful form. Microorganisms interconvert these oxyanions, and this biotransformation impacts the assembly and availability of As. Natural sources, such as geological erosion and leaching, have elevated As concentrations in the groundwater. Anthropogenic sources include As leakage from mining, metal processing, pesticide, and fertilizer production (Chung et al. 2014).

Elevated As levels in drinking water have been observed in several nations, including Argentina, Bangladesh, China, Chile, Canada, Japan, Vietnam, Taiwan, India, Mongolia, Nepal, and the United States (Smith et al. 2009). One of the worst natural disasters is groundwater poisoning due to As in India's Ganga-Brahmaputra river plains. In India, Chhattisgarh, Jharkhand, Bihar, West Bengal, and Uttar Pradesh in the Ganga river flood plain, Assam and Manipur in the Brahmaputra and Imphal river flood plains are heavily contaminated with As. Figure 1 shows India's major arsenic-contaminated sites.

In India, As contamination in the groundwater of West Bengal and Bihar is a matter of great concern. The Central Pollution Control Board (CPCB) in India closely monitors the level of As pollution and the performance of the As Removal Plants (ARP) (Hossain et al. 2006). CPCB has also offered National Planning Commission regulatory measures (https://cpcb.nic.in/who-guidelines-for-drinking-water-quality/) to check the As level in the drinking water.

As pollution in identified areas of India ranges up to 10 g/L. The permissible limit of total As in drinking water as demarcated by the US Environmental Protection Agency (USEPA), World Health Organization (WHO), and Bureau of Indian Standards (BIS) are 0.01, 0.05, and 0.05 ppm, respectively. The US Agency for Toxic Substances and Disease Registry (ATSDR) has been marked As on first rank with a cumulative score of 1676 in the priority list of toxic substances.

A considerable volume of research has been done to improve understanding of As contamination in groundwater: its sources, extent, and scale of the groundwater contamination, As leaching from soil into the groundwater, and the impact of As toxicity on community health. Researchers have extensively worked on developing techniques for detecting and eliminating As from the groundwater (Ghosh and Singh 2010).

Heavy metal resistance in bacteria is mediated by five primary mechanisms: extracellular barrier, active metal ion transport (efflux), extracellular sequestration, internal sequestration, and metal ion reduction. Toxic metal resistance is a genetic mechanism found in microorganisms. Several plasmids have been discovered in halophilic bacteria, especially in the *Halomonas* genus, indicating resistance against heavy metals (Fekih et al. 2018).

The As resistance in prokaryotes requires As(V) reduction *ars*C operon, *aio*A oxidation operon, *arr*A respiratory reduction operon, As(III) transporter *ars*B operon, and As-specific methylation *ars*M gene (Sher et al. 2020). As resistance is provided by the *ars* gene system in various bacterial species. The *ars* operons are found in a wide range of bacteria. The genes arsenite inducible repressor (*ars*R), arsenite permease (*ars*B), and arsenate reductase (*ars*C), which constitute most operons,

have been extensively studied (Ordóñez et al. 2005). The *ars* operons found in *Escherichia coli*, *Pseudomonas aeruginosa*, and *Staphylococcus* species contain the genes *ars*RDABC (Branco et al. 2008). *ars* operons are more numerous than tryptophan biosynthesis genes in most of the bacterial genomes. The *ars*C reduces As(V), and its primary detoxifying activity is the expulsion of As(III) from the cell via an As(III) efflux pump (*ars*B) (Inskeep et al. 2007). The partial gene sequence in 250 bp amplicons has shown the amplification for As(V) reductase, specifying the efflux mechanism (Sher et al. 2020).

Jain et al. (2011) reported that *Bacillus cereus* strain AG27 isolated from the soil carries the *ars*C gene, having resistance against As(V) by converting it to As(III) and subsequently ejecting it out of the cell. The strain had minimal inhibitory concentrations (MIC) of 40 and 35 mM for As(V) and As(III), respectively. *arr* operon-containing bacteria utilize As(V) as an electron acceptor and convert it to more soluble and toxic As(III). The *arr*A gene is highly conserved and is required for As(V) respiration (Malasarn et al. 2004). As(V) acts as a phosphate analog, preventing the uptake and utilization of phosphate. As(V)-based minerals are commonly considered as a subclass of phosphate minerals due to their similar size and charge. Owing to this resemblance, As(V) minerals are found in a wide range of As-rich soils and oxidized environmental settings (Sher et al. 2020).

As(V) is less toxic than As(III), and several bacterial species oxidize As(III) during detoxification. The main *aio*A gene, also known as *aox*B, *aso*A, and *aro*A, is responsible for As(III) transformation by oxidation (Escudero et al. 2013).

This study aims to isolate highly As-resistant bacteria from the contaminated site. Coevolved genes are explored to determine gene expressions that contribute to resistance mechanisms. Additionally, biochemical and morphological characterization of the isolate are also done to assess its As(III) and As(V) removal efficiency.

2 | Materials and Methods

2.1 | Sample Collection and Isolation of Microorganisms

The contaminated water samples were collected from the Ramnagar Fort, Ganga River, Varanasi (location coordinates: 25.27097 N 83.02350 E), Uttar Pradesh, India, in December 2021. The water samples were collected and preserved as per standard American Public Health Association (APHA) guidelines. The water sample was vortexed, and the pellet was inoculated in the nutrient broth at 37°C and 180 rpm for 24 h. The inoculum was plated on the same medium, and the recovered morphotypes were purified.

2.2 | As Stock Preparation

The stock solution of sodium arsenite (1000 ppm) ($NaAsO_2$, mol.wt. −129.91 assay purity: 98%; Otto, India) and sodium arsenate dibasic heptahydrate ($Na_2HAsO_4.7H_2O$, mol.wt. −312.01, assay purity: 98.50%–102.0%; HiMedia, India) were prepared by adding 1.73 g of $NaAsO_2$ and 4.16 g of $Na_2HAsO_4.7H_2O$ in 1 L of distilled water. All of the chemicals and reagents used in experiments were of the analytical reagent (AR) grade.

2.3 | Screening of Bacterial Isolates

The isolates were assessed qualitatively on the nutrient broth media to screen As-resistant strain. 10 ppm of $Na_2HAsO_4.7H_2O$ and $NaAsO_2$ was added to broth containing mid-log phase cells of isolates. The cells were incubated at 37°C for 24 h. Hydrolytic zones were observed around the bacterial colonies. The most promising isolates were selected for further investigation. All experiments were done thrice, and the average of the observations was recorded.

Quantitative screening of the positive isolates was performed to determine As resistance. Inoculated medium spiked with As(III) and As(V) was separately incubated overnight at 37°C. After centrifugation of 10,000 g for 10 min, the crude bacterial pellets were extracted and tested for 10–4000 ppm concentrations.

2.4 | Bacterial Isolate Identification by 16S rRNA Amplification

A genomic DNA template was extracted from the bacterial culture using a genomic DNA isolation kit (Qiagen, Germantown, Maryland, USA). Primers 5′-TCCTACGGGAGGCAGCAG-3′ and 5′-GGCGGTGTGTACAAGGCCC-3′ were used to amplify the 16S rRNA gene by polymerase chain reaction (PCR). Detailed information has been given in Section S1.1 of the Supporting Information.

2.5 | MIC of Bacterial Isolate

In a 50-mL conical flask, 25 mL of nutrient broth (NB) (HiMedia Laboratories Private Limited, Mumbai, India) was poured. $Na_2HAsO_4.7H_2O$ and $NaAso_2$, ranging from 10 to 4000 ppm and 10 to 3000 ppm, were added, respectively. Reaction mixtures were inoculated and kept on shaking-cum-incubation at 180 rpm for 24 h at 37°C. Detailed information has been given in Section S1.2 of the Supporting Information.

2.6 | Growth Condition for Isolate

After being grown on NB medium, the strain was kept at 37°C overnight. The mid-log phase cells were picked up from nutrient broth, streaked on nutrient agar plates, and stored at 4°C for later use. Detailed information on genomic DNA isolation from culture is given in Section S1.3 of the Supporting Information.

2.7 | PCR Amplification of As-Resistant Gene

The As resistance gene was amplified using a template of the isolated DNA. Detailed information has been given in Section S1.4 of the Supporting Information. PCR conditions for *ars*C, *ars*M, *aio*A, and *arr*A Gene amplification have been given in Section S1.5 of the Supporting Information.

2.8 | Scanning Electron Microscopy (SEM)

Scanning electron microscopy (SEM) (Nova Nano SEM 450, USA) microanalysis system was used to study bacterial isolate's morphological characteristics and cell size (Bunnoy et al. 2019). The isolate was grown in NB broth (control) spiked with 1000 ppm As(V) and As(III) under optimal growth conditions. The bacterial broth was centrifuged at 3000 rpm for 5 min to obtain the pellet. The pellet was washed thrice with buffer saline PBS (pH 7.4) to remove the impurities. The cells were fixed for 20 min at room temperature with glutaraldehyde (3%). The fixed cells were rinsed in PBS buffer twice before being dehydrated. The dehydration of fixed cells was done in an environment of ethanol at dilutions 30%, 50%, 70%, and 100% with 10 min of incubation intervals. The cells were suspended on the glass slides by pouring 2–3 drops and dried at room temperature.

2.9 | Elemental Mapping and Energy-Dispersive Spectroscopy (EDS) Analysis

Elemental analysis of surfaces in SEM was performed by energy-dispersive spectroscopy (EDS) (TEAM Pegasus Integrated EDS-EBSD with Octane Plus and Hikari Pro, EDAX Inc.). Isolated As-resistant bacterial culture was grown in control, and different As concentration samples were isolated from broth and lyophilized to achieve the dried powdered sample before being evaluated in SEM-EDS.

2.10 | X-Ray Diffraction (XRD)

Dried cell powder of 0.2 g was scattered across the testing plates. Diffractometers with Cu-K radiation having a wavelength of 1.54 Å were used to scan the sample. The angle 2θ in the x-ray diffraction (XRD) setup was in the range of 10°–90°.

2.11 | Fourier Transformed Infrared (FTIR)

The isolate was cultivated for 24 h in As(III) and As(V) stress and Control. After 10 min of centrifugation at 3000 rpm, the pellet was collected. The pellet was rinsed multiple times in regular saline before being freeze-dried overnight. The dry pellet was pulverized in the presence of KBr. Infrared spectra (IR) (Shimadzu, Japan) were captured in the 4000–400 cm^{-1} range (Sher et al. 2020).

3 | Results and Discussion

3.1 | Phylogenetic Analysis

Figure 2 shows the phylogenetic tree of *Acinetobacter junii* MKVVM4 IITBHU with its closest strains. Alignment of full-length sequences was made with ClustalW (MEGA 11). The maximum likelihood method with a scale length of 0.05 was used to obtain the phylogenetic tree. The strain closest to *A. junii* MKVVM4 IITBHU was found to be *A. junii* PPS-16 from one cluster. However, *A. junii* DKD and *Acinetobacter* CHBE-M6 had 99.10% similarity in another cluster.

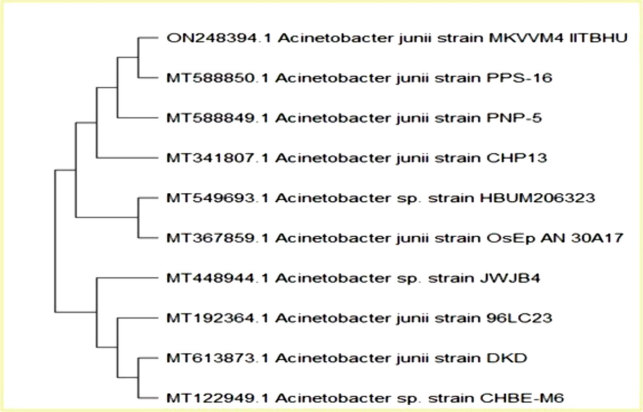

FIGURE 2 | Phylogenetic tree of *Acinetobacter junii* MKVVM4 IITBHU.

The closest relatives of *A. junii* MKVVM4 IITBHU according to genetic distance are the *Acinetobacter* sp. HBUM206323 (1.12) and *A. junii* PPS-16 (1.94). High sequence conservation and recent evolutionary divergence are suggested by the incredibly low divergence (0.00003) found by genetic distance analysis. *A. junii* MKVVM4 IITBHU exhibits less evolutionary divergence when compared to other isolates in the collection. The genetic distances of the other *A. junii* isolates varied, with the majority falling below 2.0, indicating a generally close evolutionary relationship within the species.

The 16S rRNA sequence *A. junii* MKVVM4 IITBHU was submitted to NCBI, USA, and accession no. ON248394 was allotted. The gyrB sequence homology of the *Acinetobacter* strain ranged from 69.6% to 99.7%, making them a highly developed taxonomic group as compared to the genetic distance between *Pseudomonas putida* IFO 14164T and *E. coli* K-12 (74.6% identity) (Yamamoto and Harayama 1996).

3.2 | Gram Staining

Figure 3a–c shows the Gram-stained images of *A. junii* MKVVM4 IITBHU.

Figure 3a–c depicted that isolated *A. junii* MKVVM4 IITBHU was Gram-negative. The bacterial cells were Gram-negative aerobic bacteria with a coccobacillus structure. The life cycle significantly impacts the appearance of *Acinetobacter* species, making it distinct from other microbial species when seen with a Gram stain. *Acinetobacter* species appeared to be rod-shaped in their early stages of growth. The cells developed a coccobacillary morphology in the stationary phase. However, the non-motility of *A. junii* MKVVM4 IITBHU is questionable (Bonomo 2012).

3.3 | Redox Property

As(III) oxidation and As(V) reduction by *A. junii* MKVVM4 IITBHU was demonstrated by the development of colored complexes on the growth plate (Figure 4). White color development in control reflected that no colored compounds of As species have formed. The As transformation assay demonstrated

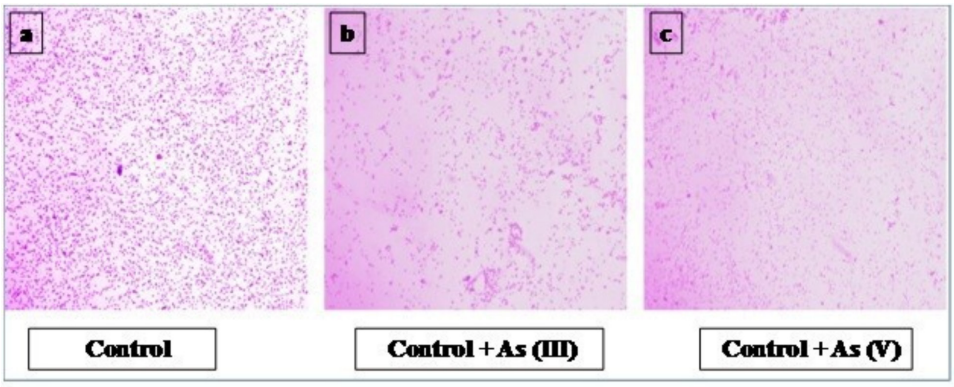

FIGURE 3 | Gram staining of *Acinetobacter junii* MKVVM4 IITBHU. (a) Control. (b) Control + As(III). (C) Control + As(V).

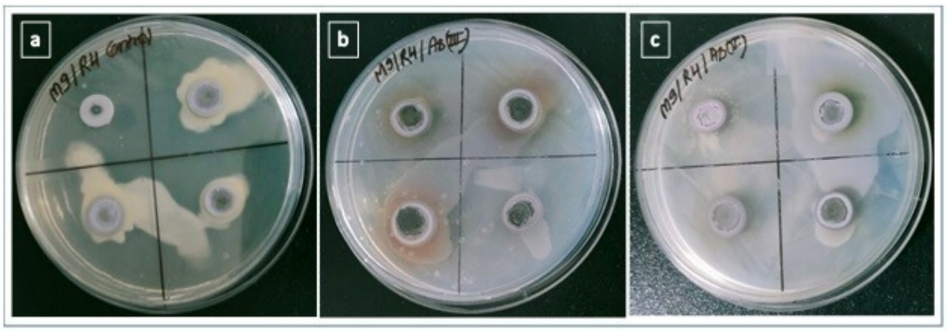

FIGURE 4 | *Acinetobacter junii* MKVVM4 IITBHU phenotypic detection of (a) control, (b) control + As(III), and (c) control + As(V) plate incubation with $AgNO_3$.

TABLE 1 | Biochemical and morphological characteristics.

Biochemical and morphological tests	Results
Shape	Coccobacilli
Gram staining	−ve
Catalase	+ve
Nitrate reduction	+ve
Oxidase	−ve
Indole	−ve
H_2S production	−ve
Voges–Proskauer (VP)	−ve
Urease	−ve
Lactose fermentation	−ve

effective oxidation of As(III) and reduction of As(V) by *A. junii* MKVVM4 IITBHU. The oxidation of As(III) to As(V) was recorded by the emergence of a dark brown-red As(III) precipitate. In contrast, As(V) was converted to As(III) because a light yellow precipitate appeared.

Simeonova et al. (2004) demonstrated that the detection of As(III) oxidizers and As(V) reducers by the $AgNO_3$ colorimetric approach was accurate and sensitive over a wide pH range (5.8–8.4). It has been suggested that screening libraries can do semiquantitative testing of isolates to explore genes involved in the oxidation or reduction of As.

3.4 | Biochemical Characterization

Table 1 shows the biochemical characteristics of *A. junii* MKVVM4 IITBHU.

It was observed that *A. junii* MKVVM4 IITBHU was non-motile, aerobic, non-lactose fermenting, catalase positive, non-fastidious, and oxidase negative. Similar findings have been reported by Bonomo (2012) and Constantiniu et al. (2004).

3.5 | Growth Curve

Figure 5 shows the growth curve of *A. junii* MKVVM4 IITBHU in control and As stress.

The *A. junii* MKVVM4 IITBHU growth expanded rapidly in the initial 4–6 h on the As(V) medium compared to the control. This demonstrated that bacteria attained maximal growth in the first 12 h under As(III) stress. Bacteria grew very slowly and entered the stationary phase at 14 h. *A. junii* MKVVM4 IITBHU under As(V) endured a lengthy period at high concentrations of As to establish a diauxic growth mechanism of detoxifying As. Growth patterns showed that *A. junii* MKVVM4 IITBHU utilized oxidation or reduction of the toxic As for metabolic activity when exposed to As(III) and

As(V). The *A. junii* MKVVM4 IITBHU showed an increased growth rate till the first 20 h in As(III) and As(V), indicating that the bacteria developed a tolerance as they were able to grow more readily at higher concentrations of As. As located beneath phosphate (P) in the periodic table, which is a chemical analog of P. As it has an atomic radius and electronegativity almost equal to the P. Arsenate (AsO_4^{3-}) behaves similarly to phosphate (PO_4^{3-}). The GFAJ-1 was viable in the high-As concentration in the Mono Lake of California without PO_4^{3-} metabolism. The authors have also claimed that As replaced PO_4^{3-} in the bacterium biomolecules (Wolfe-Simon et al. 2011). Basturea et al. (2012) also illustrated that As(V) worked as a phosphate molecule in the extensive breakdown of ribosomes. A lengthy lag time in a + As/-P-based medium allowed a small number of As(V) tolerant cells to survive.

3.6 | Minimum Inhibitory Concentration (MIC)

A. junii MKVVM4 IITBHU showed high resistance against both As(III) and As(V) forms. The strain had MIC of 4000 and 3000 ppm for As(V) and As(III), respectively. No growth was observed at 4000 ppm of As(III). However, growth was observed at 4000 ppm of As(V) in 24 h. Delayed bacterial growth was observed at 3000 ppm As(III) containing medium after 24 h.

Table 2 shows a comparative As(III) and As(V) tolerance level study of *A. junii* MKVVM4 IITBHU with the other bacterial strains.

A. junii MKVVM4 IITBHU showed a significantly higher tolerance level of 3000 ppm for As(III) than other bacterial isolates reported in the literature.

Arsenic oxidation state changes are a crucial detoxifying mechanism carried out by *A. junii* MKVVM4 IITBHU. Arsenate reductase enzymes that selectively catalyze the reduction of As(V) to As(III), which can thereafter be further expelled or sequestered by the bacterial cell, are probably responsible for supporting the reduction process. The isolate able to survive exposure to arsenic through oxidation state changes and other physiological adaptations. Data illustrating the isolate's growth curves in the presence of arsenic at different concentrations were produced by the experiment. At quantities that would often prevent the growth of other bacterial isolates, the isolate's growth remains unaffected, demonstrating a notable resistance to arsenic concentrations up to 4000 ppm.

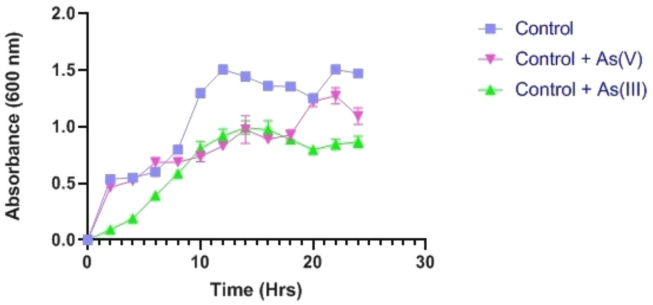

FIGURE 5 | Growth curve of *Acinetobacter junii* MKVVM4 IITBHU.

3.7 | PCR Products and Gene Amplification

Figure 6 shows *ars*C gene amplification. Lanes 2 and 3 show amplifications from the genomic DNA of control. Lanes 4, 5, and 6 represent amplifications from the genomic DNA under As(III) 3000 ppm, As(III) 4000 ppm, and As(V) 4000 ppm, respectively. A 100 bp ladder in Lane 1 clearly shows that the amplified gene *ars*C was approximately 300 bp in length. Lanes 3 and 6 show high-quality *ars*C gene amplification. Figure 6 also showed that control and 4000 ppm As(V) provided a suitable environment for the *ars*C gene.

Tsuchiya et al. (2019) showed that 0.1 μM As(III) enhanced the expression of *arr*A. This improved the expression of the detoxifying As(V) reductase gene *ars*C.

The GenBank sequences for *ars*C were 414 and 492 bp long for *Klebsiella* and *Yersinia enterocolitica*, respectively (Sun et al. 2004). In the present work, the amplified *ars*C gene isolated from the *A. junii* MKVVM4 IITBHU had a length of about 300 bp. The disparity in base pair lengths was due to different bacterial isolates used in studies.

Figure 7 shows gradient PCR amplified *ars*M gene products electrophoresed on the agarose gel. Lane 5, 6, and 7 obtained at 48°C, 49°C, and 50°C show the successful amplification of the *Ars*M gene. The low amplified products of *ars*M were observed in Lanes 2, 3, and 4 at 52°C, 53°C, and 54°C. The 100 bp ladder in Lane 1 showed that the amplified gene *ars*M was approximately 350 bp in length. The PCR products from genomic DNA isolated

TABLE 2 | Tolerance level against As(III) and As(V).

Microorganism	As(III) (ppm)	As(V) (ppm)	References
Mycobacterium smegmatis	74.92	1873	Ordóñez et al. (2005)
Staphylococcus aureus	149.84	3746	Ordóñez et al. (2005)
Nocardia corynebacteroides	149.84	7492	Ordóñez et al. (2005)
Bacillus subtilis	187.3	5619	Ordóñez et al. (2005)
Streptomyces lividans	299.7	11,238	Ordóñez et al. (2005)
Acinetobacter xylosoxidans BHW-15	1123.8	—	Diba et al. (2021)
Escherichia coli DH5α	374.6	7492	Ordóñez et al. (2005)
Pseudomonas fluorescens	449.5	14,984	Ordóñez et al. (2005)
Pseudomonas putida	524.4	14,984	Ordóñez et al. (2005)
Acinetobacter junii MKVVM4 IITBHU	3000	4000	This study

from *A. junii* MKVVM4 IITBHU depicted that lower annealing temperature facilitated the amplification of the *ars*M gene.

As(III) resistance in an As-sensitive strain of *E. coli* was demonstrated by heterologous production of *ars*M from *Rhodopseudomonas palustris*. The *ars*M catalyzed the formation of methylated intermediates to produce trimethylarsine from As(III) (Qin et al. 2006).

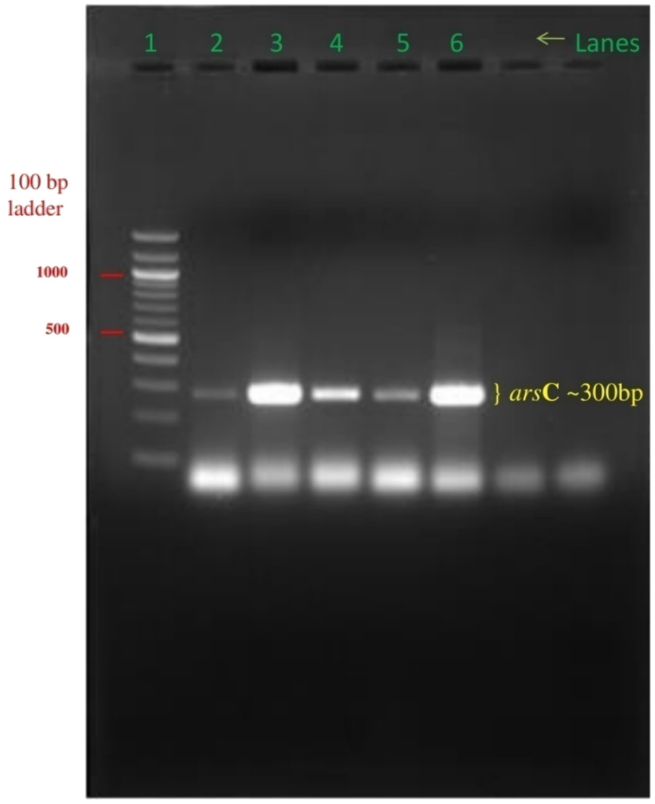

FIGURE 6 | Doc image of amplified *ars*C gene.

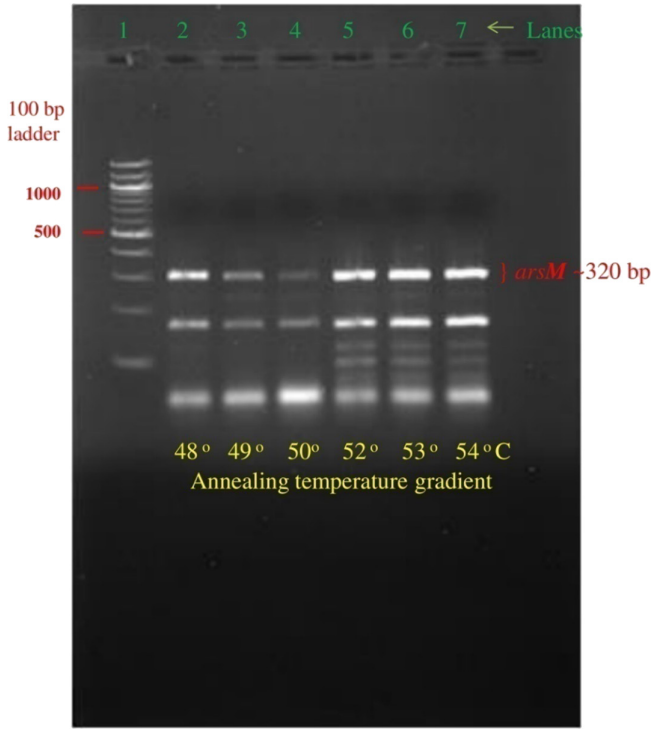

FIGURE 7 | Gel doc image of amplified *ars*M gene.

An arsenic-sensitive strain of *E. coli* was employed as a heterologous host to examine the function of the *ars*M gene in arsenite As(III) resistance. The *A. junii* MKVVM4 IITBHU containing *ars*M was evaluated for its capacity to confer resistance. These results were in line with earlier research showing that *ars*M encodes an arsenite methyltransferase, which aids in the methylation and volatilization processes necessary for arsenic detoxification. The study demonstrates the possibility of *ars*M in bioremediation applications and supports its functional role in microbial arsenic resistance.

The *aio*A gene amplification is evident in Lane 3 of Figure 8. It has a length of about 400 bp. The *arr*A gene amplification is also visible in Lane 4 of Figure 8, around 1100 bp. Lane 1 corresponds to a 100 bp ladder band to determine expressed gene base-pair length.

Understanding arsenic resistance and biotransformation pathways in microbial communities requires first amplifying the *arsC* and *arsM* genes using PCR. Important parts of the microbial arsenic detoxification mechanism are these genes. By changing toxic arsenate into less hazardous forms, arsenate reductase, which is encoded by the *arsC* gene, converts arsenate As(V) to arsenite As(III), aiding in arsenic bioremediation. Because arsenate and phosphate share structural similarities and might interfere with cellular functions, this is an essential step in the detoxification of arsenic.

Because arsenite is more readily carried across cellular membranes and can be extruded or further changed for detoxification, the reduction from As(V) to As(III) is crucial.

Arsenite S-adenosylmethionine methyltransferase, which is encoded by the *arsM* gene, methylates arsenite to produce volatile

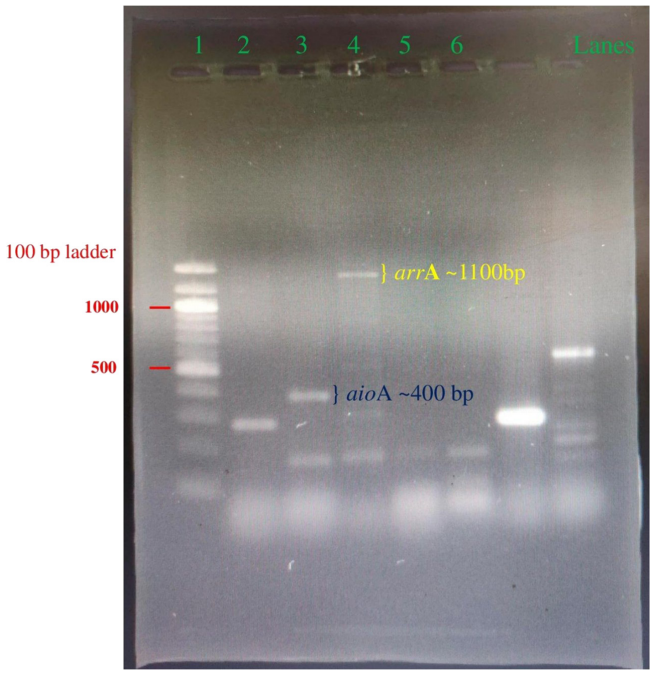

FIGURE 8 | Gel doc image of amplified *aio*A and *arr*A gene.

organic arsenic species such dimethylarsinic acid (DMA) and monomethylarsonic acid (MMA). This contributes to the global arsenic cycle and aids in the detoxification of arsenic. Rapid identification of arsenic-resistant bacteria in a variety of settings is made possible by PCR amplification of *arsC* and *arsM*, which also offers information on how microorganisms have adapted to arsenic stress. It is possible to monitor the evolution and horizontal gene transfer of arsenic resistance genes among various microbial taxa by analyzing amplified products.

Ordoñez et al. (2018) established the significance of 18 *haloarchaea* colonies regarding As tolerance by linking it to the *Halorubrum* genus. The *aio*A and *arr*A partial genes were found in 11 of 18 colonies. These genes were involved in catalyzing the oxidation and reduction of As compounds.

Suhadolnik et al. (2017) studied the *aio*A, *ars*C, and *arr*A expression. The authors observed that horizontal gene transfer took place. These genes had a high degree of sequence variation, especially in the case of *arr*A. The following species were observed as As(V)-reducers and As(III)-oxidizers: *Dechloromonas*, *Acidovorax facilis*, *Acidovorax delafieldii*, *Aquabacterium*, *Shewanella*, *Clostridium thermopalmarium*, and *Macellibacteroides fermentans*. There were divisions of OTUs into several clusters in the phylogenetic tree of *aio*A. This was due to segregation or functional gene variations.

3.8 | SEM

The cells were observed in single and densely clustered healthy cells (Figure 9). SEM images depicted that in the early growth stage, the spore head shape was like coccobacilli and the tail was rod-shaped. SEM examination revealed significant differences in size. The size of *A. junii* MKVVM4 IITBHU at a scale of 1 μm (50,000× magnification) was 2.89 μm in length and 530.52 nm in breadth.

An overview of the distribution and organization of bacterial cells is given by the top two photos, which are taken at a lower magnification. A closer look at the cell surface features and potential morphological changes is made possible by the increased magnification of the bottom two photos. The rod-shaped, homogeneous, and aggregated appearance of the bacterial cells suggests normal growth activity. Measurements (green annotations) showing the size of bacterial cells are included in the bottom-left image. According to the measurements, the cell length is consistent within a particular size range (e.g., ~3.5–5.5 μm). An even higher magnification of the bacterial surface is shown in the bottom-right image, which may show extracellular deposits or surface roughness. These pictures depict that bacterial cells subjected to arsenic stress, morphological alterations such surface roughness, elongation, or variations in aggregation would suggest that the arsenic interacted with the bacterial membrane. Extracellular deposits or structures indicated that arsenic had biomineralized or adhered to the bacterial surface. A comparison of photos using a scale bar would highlight structural differences in various scenarios.

Kushwaha et al. (2017) revealed that the cells of *A. junii* Pb1 had a smooth surface and a rod-like shape in Control. Bacterial surfaces became rough and cell thickness increased substantially at 250 ppm of Pb(II). Similarly, Dey et al. (2016) showed that the isolates SW2 and SW4 generated chain-like arrangements when exposed to As. The size of the SW2 was smaller than the control. Both isolates accumulated heavy metals.

3.9 | EDS Quantification

The results of EDS in control, control + As(III), and control + As(V) exposed cells are shown in Figure 10.

The EDS spectra's detection of As demonstrates that *A. junii* MKVVM4 IITBHU bioaccumulates it. For greater clarity, it is necessary to specifically identify the precise atomic percentage of arsenic and its relative accumulation between As(III) and As(V) circumstances. Furthermore, it is important to highlight the statistical significance of the data display. In the samples subjected to As(III) and As(V), the EDS spectra (image a) show distinct As peaks. This demonstrates that *A. junii* MKVVM4 IITBHU takes up arsenic from its supplement media and either stores it within its cells or transforms it into different forms for bioremediation. The standard deviation (SD) or standard error of the mean is shown by error bars in the bar graph. A highly significant difference in arsenic accumulation between the control and arsenic-treated samples is shown by a ***, which stands for $p < 0.001$. The atomic percentage of arsenic increased significantly in the As(III) condition, indicating that *A. junii* is more capable of bioaccumulating As(III) than As(V). The idea that *A. junii* preferentially accumulates As(III), possibly as a result of variations in absorption processes and transport efficiency, is strongly supported by our data and point to a species-specific resistance mechanism.

Elemental profiling revealed significant variations in the atomic proportion of key elements in response to arsenic treatment. The control group had higher levels of nitrogen (N) and carbon (C), which are often associated with organic and proteinaceous content. After being exposed to arsenic, especially at the higher dose (control + AsV), a notable reduction in the amount of carbon and nitrogen was seen. This decline may be the consequence of oxidative biomolecule destruction or inhibition of metabolic pathways involved in production. The concentrations of minor elements such as silicon (Si), aluminum (Al), magnesium (Mg), and sodium (Na) were relatively stable throughout all groups, with only modest changes. As expected, successful exposure was confirmed by the greater arsenic (As) levels in the treated groups.

In comparison to control and control + AsV, a significant drop in carbon and nitrogen was seen in the control + AsIII group, indicating potential degradation or structural change of carbonaceous and nitrogen-containing biomolecules at this concentration. On the other hand, the control + AsV group's oxygen concentration rose noticeably, which might be a result of oxidative stress or the buildup of oxygen-rich compounds in reaction to increasing arsenic exposure. There were also statistically significant differences between silicon and sodium.

Nine crucial elements, namely, C, O, N, Na, Mg, As, Al, Si, and P, were observed in EDS. However, other nonessential elements, Pb and Al, were also observed in the spectra. This reflected that

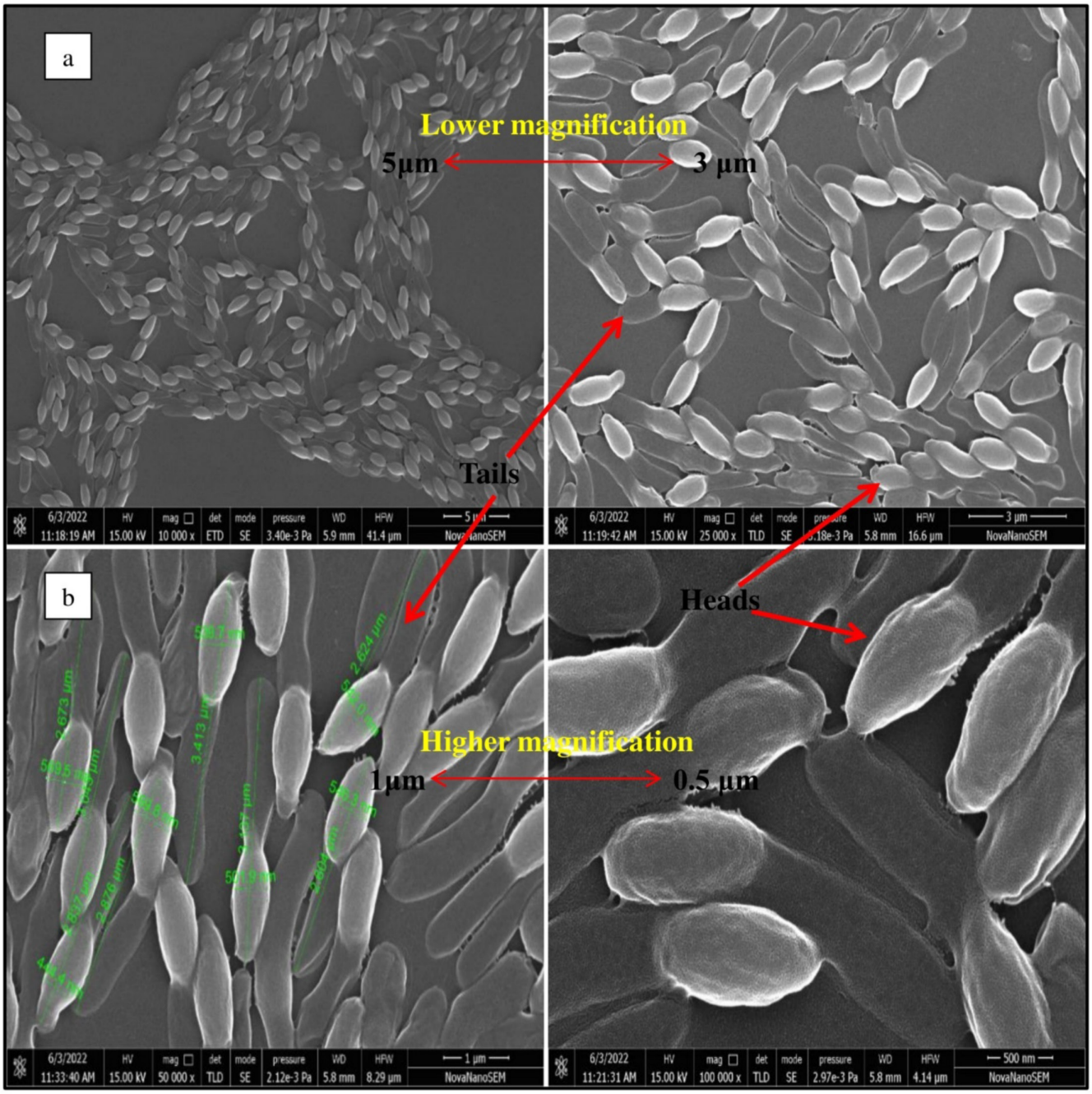

FIGURE 9 | SEM image of isolate. (a) Top image of lower magnification at scale of 5 and 3 µm. (b) Bottom image of higher magnification at scale of 1 and 0.5 µm.

these elements were utilized in metabolism for energy generation and bacterial growth. Si, O, Na, C, and N were the major constituents, accounting for approximately 81% of the total elemental mass of bacterial biomass. The presence of As in EDS spectra showed its bioaccumulation in the *A. junii* MKVVM4 IITBHU.

3.10 | XRD

The *A. junii* MKVVM4 IITBHU in control, As(III), and As(V) medium was observed by the XRD pattern at $2\theta = 20°$ (Figure 11). Broad diffraction peaks from 14° to 36° were typically observed as strain lacked a crystalline phase and had a disordered structure. Significant intensity variations were noted between 2500–8000 counts. The amorphous hump was seen in the control at 20.479°, displaced to 22.486° in As(III) exposed *A. junii* MKVVM4 IITBHU. The difference in intensity count was represented at 6862.06 and 5215.38 counts, respectively. *A. junii* MKVVM4 IITBHU exposed to As(V) displayed two crystalline peaks with intensities of 5350.84 and 4673.50 count 26.50° and $2\theta = 29.42°$, respectively. It became evident from these amorphous hump shifts and distinctive peaks that the adsorption of As on bacterial cell surface was responsible for these modifications.

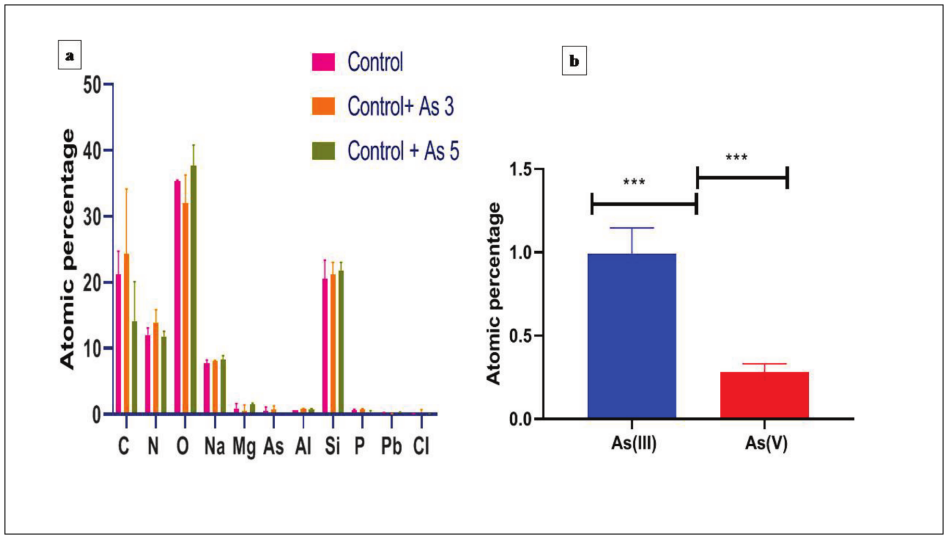

FIGURE 10 | Quantitative analysis of the elemental composition by (a) control along with As(III) and As(V) and (b) atomic percent of As.

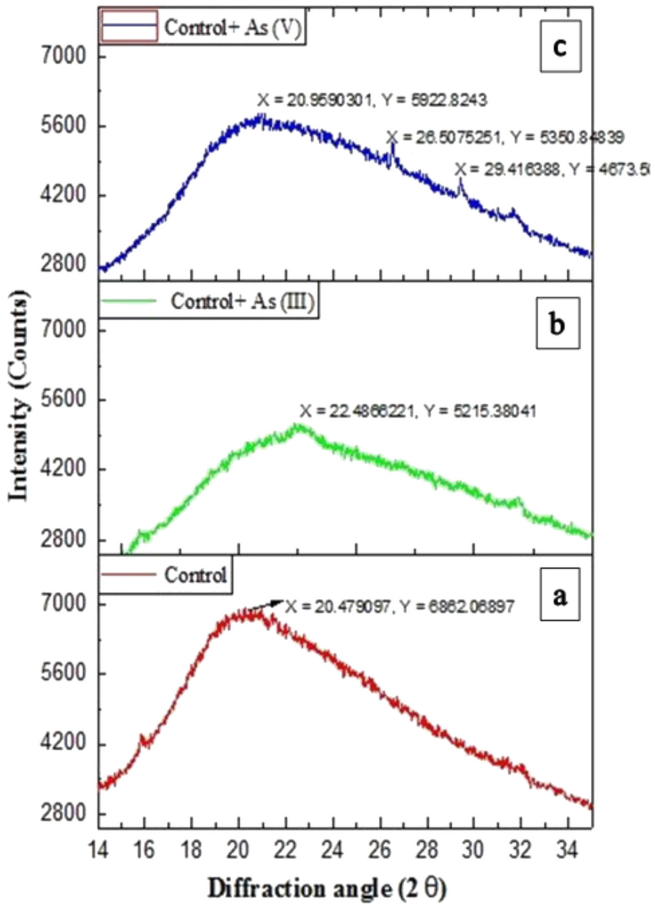

FIGURE 11 | XRD pattern of (a) control, (b) control + As(III), and (c) control + As(V).

Garai et al. (2020) claim that the large humps observed between 15° and 35° indicate towards amorphous nature of the samples. Uppal et al. (2016) examined the XRD pattern of commercial synthetic graphite (SG), which exhibited a strong diffraction peak at 26.3° and a d-spacing of 0.336 nm at 002 planes (JCPDS no. 25-0284). The XRD pattern of functionalized synthetic graphite also showed the surface adsorption of As. In addition to this, FSG-As also displayed classical As peaks at 50.1° and 63.1°.

The structural changes brought on by arsenic (As) adsorption onto the bacterial cell surface are indicated by changes in amorphous humps and characteristic peaks in XRD patterns. Interactions between As and surface biomolecules cause these modifications, which result in changes to amorphous areas (broadening or intensity changes) and variations in interplanar spacing (peak shifts). Initial evidence of these adsorption-induced structural changes was observed in comparative XRD study visible in figures of control, As(V), and As(III) peaks.

3.11 | FTIR

When *A. junii* MKVVM4 IITBHU was exposed to As most of the peaks got shifted and sharpened as compared to the control (Figure 12).

A peak shift in the region of 3384.97 (control) to 3404.41 cm^{-1} of As(III) exposed *Acinetobacter junii* MKVVM4 IITBHU signified the involvement of N–H stretching of primary aliphatic amine and −OH stretching of the alcohol. The movement of peaks from 2927.90 to 2929.14 cm^{-1} in As(III) depicted the presence of alkyl $-CH_3$, showing that an alkyl group was directly attached to the As through a carbon atom during bioalkylation carried out on the surface of *A. junii* MKVVM4 IITBHU (Bentley and Chasteen 2002).

The change of peaks from 1653.89 (control) to 1663.94 cm^{-1} in As(V) exposed *A. junii* MKVVM4 IITBHU signified the vibrations of C=O, amide, O-amino- or o-hydroxy aryl ketones and *N,N*-amide. Table 3 shows the transition of functional groups in As(III) and As(V) exposed *A. junii* MKVVM4 IITBHU.

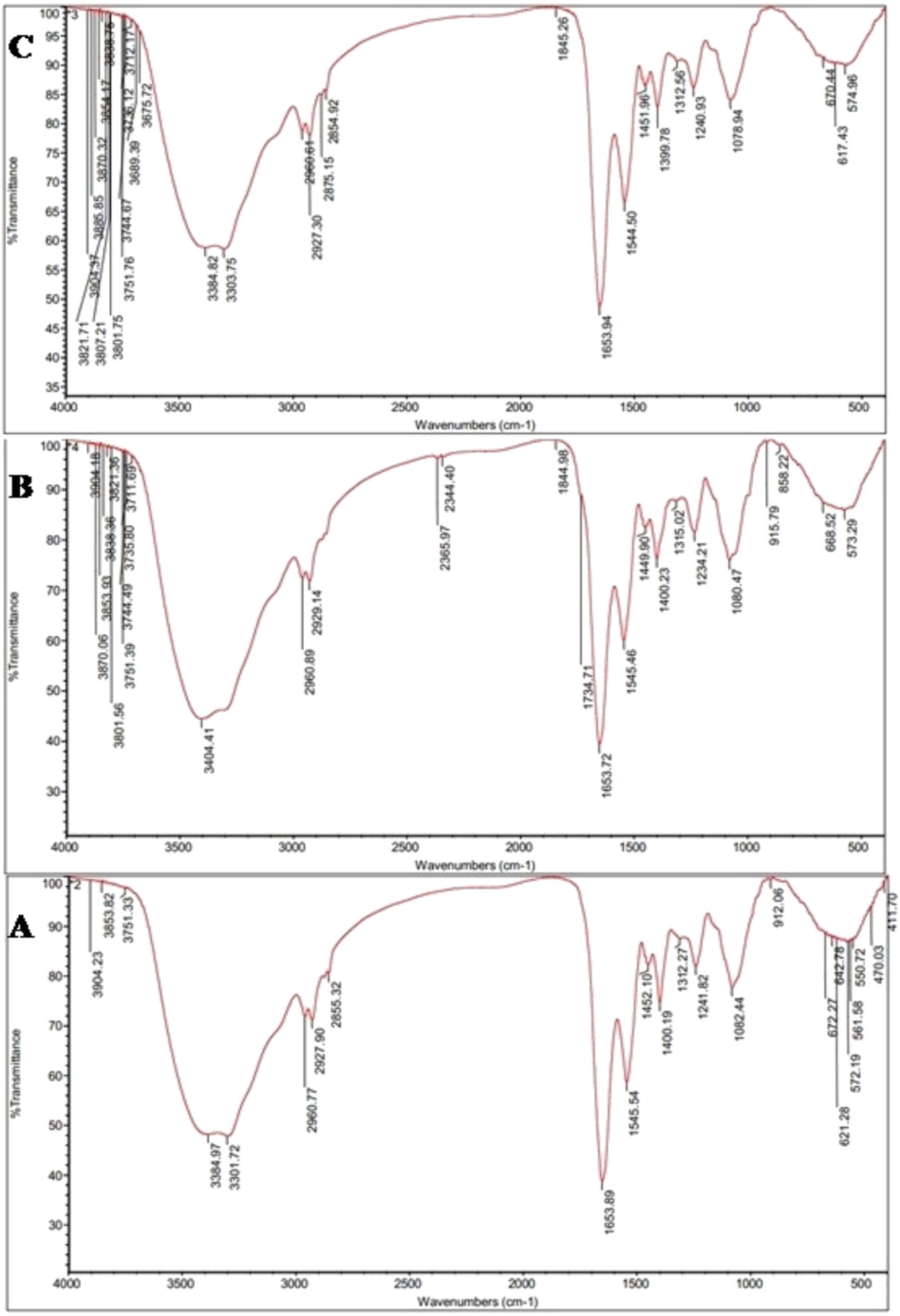

FIGURE 12 | FTIR spectrum of (A) control, (B) control + As(III), and (C) control + As(V).

As(III) and As(V) exposed *A. junii* MKVVM4 IITBHU showed a peak shift from 1452.10 to 1449.90 $cm^{-1}$and 1451.96, depicting an important role of C–H and CH_3 stretching in As binding. As(III) exposed *A. junii* MKVVM4 IITBHU also showed a transition from 1312.27 to 1315.02 cm^{-1}. This was due to As(III) binding with the surface group such as C–O, ester, carboxylic acid, anhydride, C–F (alkyl), and −OH.

In the present work, the peak transition from 1241.82 to 1234.21 cm^{-1} in As(III) and 1240.93 in As(V) exposed cells indicated towards cell wall–bound aliphatic amine and alkenes. Polysaccharides present within the cell wall were found to be involved in As(III) interaction.

The transitions from 672.27 to 668.52 cm^{-1} in As(III) and 670.44 cm^{-1} in As(V) were attributed to aromatic bending and alkyl vibrations. The peak transitions at 572.19 to 573.29 cm^{-1} in As(III) and 574.96 cm^{-1} in As(V) were due to As–O stretching vibrations.

A. junii MKVVM4 IITBHU showed the interaction between As and surface functional groups like hydroxyl, methyl, carboxyl,

TABLE 3 | FTIR of control and As(III) and (V) exposed *Acinetobacter junii* MKVVM4 IITBHU.

Wavenumber (cm^{-1})			
Control	**Control + As(III)**	**Control + As(V)**	**Functional group**
3384.97	3404.41	3384.32	N–H stretching of aliphatic primary amine and −OH stretching of alcohol
2927.90	2929.14	2927.30	Alkyl $-CH_3$ group
1653.89	1653.72	1663.94	C=O, amide, O-amino- or o-hydroxy aryl ketones, *N,N*-disubstituted amides
1452.10	1449.90	1451.96	C–H, $-CH_3$
1312.27	1315.02	1312.56	C–O, ester, carboxylic acid, anhydride, C–F (alkyl), and −OH
1241.82	1234.21	1240.93	C–O, ester, C–N amine, and C–F (alkyl, aromatic)
1082.44	1080.47	1078.94	C–O, ester, and C–Cl (aromatic)
672.27	668.52	670.44	C–Cl (alkyl), C–Br (alkyl)
572.19	573.29	574.96	C–Cl (alkyl), C–Br (alkyl)

and amino. Singh et al. (2016) obtained similar results, and Nigam et al. (2013) confirmed the changes in *Hermaea verticillata* surface morphology with modifications in functional groups after metal chelation.

4 | Conclusion

A. junii MKVVM4 IITBHU (accession no. ON248394) isolated from the Ganga River, Varanasi, U. P, India, showed hypertolerance towards As(III) and As(V). At PCR amplification annealing temperature of 53°C, the amplified genes *ars*C and *ars*M were 300 and 350 bp, respectively. It was found that the *arr*A gene participated in anaerobic respiration utilizing As(V) as an electron acceptor. During amplification, it was observed that the *ars*C, *ars*M, *aio*A, and *arr*A genes were highly conserved.

A. junii MKVVM4 IITBHU showed coccobacillus-type morphology. Additionally, it showed a tailed structure during the early stage of growth. As(V) was selected by *A. junii* MKVVM4 IITBHU as the preferred substrate for the metabolic activity required in the tolerance mechanism during diauxic development. The incremental growth of *A. junii* MKVVM4 IITBHU after 20 h in As(III) and As(V) was followed by a decline phase.

Physicochemical characterization validated the efflux of As(III) and As(V). Under different concentrations of As, there were significant changes in bacterial morphology. Negatively charged surface functional groups like −OH and −NH were involved in As(III) and As(V) biosorption. *A. junii* MKVVM4 IITBHU oxidizing, reducing, methyltransferase, and respiring gene expressions suggested that it can play an essential role in the biogeochemical cycle of As.

In this work, *A. junii* MKVVM4 IITBHU (accession no. ON248394), which was isolated from the Ganga River in Varanasi, India, was examined for its mechanisms of tolerance and As resistance. With minimum inhibitory concentrations (MICs) of 3000 ppm for As(III) and 4000 ppm for As(V), the bacterium demonstrated an extraordinarily high tolerance to arsenic contamination, outperforming the resistance levels of several previously investigated bacterial isolates. The isolate's extended survival in high arsenic concentrations supports its preference for As(V) as a substrate for metabolic processes. Two important arsenic resistance genes, *ars*C and *ars*M, which are essential for arsenic detoxification, were found by molecular characterization utilizing PCR amplification. The genes' participation in arsenic biotransformation was confirmed by their effective amplification under various arsenic environments. EDS and SEM demonstrated clear morphological alterations and changes in elemental composition in *A. junii* MKVVM4 IITBHU under arsenic stress. Overall, the results indicate that *A. junii* MKVVM4 IITBHU has a special set of physiological, biochemical, and genetic processes that allow it to live and break down arsenic in extremely polluted settings. The isolate has the potential to be used in bioremediation techniques meant to reduce arsenic pollution in aquatic environments because of its high resistance levels and capacity for arsenic detoxification. Our knowledge of its function in the biogeochemical cycle of arsenic may be improved by additional research on its metabolic pathways and genetic regulation.

Author Contributions

Manoj Kumar Verma: conceptualization, writing – original draft, writing – review and editing. **Vishal Mishra:** supervision, writing – review and editing.

Acknowledgments

The authors of the manuscript are thankful to the Indian Institute of Technology (BHU) Varanasi, India, for extending their technical and financial support.

Conflicts of Interest

The authors declare no conflicts of interest.

Data Availability Statement

The authors confirm that the data supporting the findings of this study are available within the article and its supplementary materials.

References

Basturea, G. N., T. K. Harris, and M. P. Deutscher. 2012. "Growth of a Bacterium That Apparently Uses Arsenic Instead of Phosphorus Is a Consequence of Massive Ribosome Breakdown." *Journal of Biological Chemistry* 287: 28816–28819.

Bentley, R., and T. G. Chasteen. 2002. "Microbial Methylation of Metalloids: Arsenic, Antimony, and Bismuth." *Microbiology and Molecular Biology Reviews* 66: 250–271.

Bonomo, R. 2012. "Diseases Caused by *Acinetobacter* and *Stenotrophomonas* Species." In *Goldman's Cecil Medicine*, vol. 2, 24th ed., 1881–1884. Elsevier.

Branco, R., A. P. Chung, and P. V. Morais. 2008. "Sequencing and Expression of Two Arsenic Resistance Operons With Different Functions in the Highly Arsenic-Resistant Strain *Ochrobactrum tritici* SCII24T." *BMC Microbiology* 8: 1–12.

Bunnoy, A., U. Na-Nakorn, P. Kayansamruaj, and P. Srisapoome. 2019. "*Acinetobacter* Strain KUO11TH, a Unique Organism Related to *Acinetobacter pittii* and Isolated From the Skin Mucus of Healthy Bighead Catfish and Its Efficacy Against Several Fish Pathogens." *Microorganisms* 7, no. 11: 549. https://doi.org/10.3390/microorganisms7110549.

Chung, J. Y., S. do Yu, and Y. S. Hong. 2014. "Environmental Source of Arsenic Exposure." *Journal of Preventive Medicine and Public Health* 47, no. 5: 253–257. https://doi.org/10.3961/jpmph.14.036.

Constantiniu, S., A. Romaniuc, L. S. Iancu, R. Filimon, and I. Taraşi. 2004. "Cultural and Biochemical Characteristics of *Acinetobacter* spp. Strains Isolated From Hospital Units." *Journal of Preventive Medicine* 12, no. 3–4: 35–42.

Dey, U., S. Chatterjee, and N. K. Mondal. 2016. "Isolation and Characterization of Arsenic-Resistant Bacteria and Possible Application in Bioremediation." *Biotechnology Reports* 10: 1–7.

Diba, F., M. Z. H. Khan, S. Z. Uddin, et al. 2021. "Bioaccumulation and Detoxification of Trivalent Arsenic by Achromobacter Xylosoxidans BHW-15 and Electrochemical Detection of Its Transformation Efficiency." *Scientific Reports* 11: 21312.

Escudero, L. V., E. O. Casamayor, G. Chong, C. Pedrós-Alió, and C. Demergasso. 2013. "Distribution of Microbial Arsenic Reduction, Oxidation and Extrusion Genes Along a Wide Range of Environmental Arsenic Concentrations." *PLoS ONE* 8, no. 10: e78890.

Fekih, I. B., C. Zhang, Y. P. Li, et al. 2018. "Distribution of Arsenic Resistance Genes in Prokaryotes." *Frontiers in Microbiology* 9: 2473. https://doi.org/10.3389/fmicb.2018.02473.

Garai, M., C. H. V. Rao, and B. Karmakar. 2020. "Nanocrystalline Microstructure in Sm^{3+} and Gd^{3+} Doped K_2O–MgO–Al_2O_3–SiO_2–F Glass-Ceramic Sealant (SOFC)." *Materials Advances* 1, no. 3: 463–468. https://doi.org/10.1039/D0MA00179A.

Ghosh, N. C., and R. D. Singh. 2010. "Groundwater Arsenic Contamination in India: Vulnerability and Scope for Remedy."

Hossain, M. A., A. Mukharjee, M. K. Sengupta, et al. 2006. "Million Dollar Arsenic Removal Plants in West Bengal, India: Useful or Not?" *Water Quality Research Journal* 41: 216–225.

Inskeep, W. P., R. E. Macur, N. Hamamura, T. P. Warelow, S. A. Ward, and J. M. Santini. 2007. "Detection, Diversity and Expression of Aerobic Bacterial Arsenite Oxidase Genes." *Environmental Microbiology* 9: 934–943.

Jain, S., B. Saluja, A. Gupta, S. S. Marla, and R. Goel. 2011. "Validation of Arsenic Resistance in *Bacillus cereus* Strain AG27 by Comparative Protein Modeling of arsC Gene Product." *Protein Journal* 30: 91–101.

Kushwaha, A., R. Rani, S. Kumar, T. Thomas, A. A. David, and M. Ahmed. 2017. "A New Insight to Adsorption and Accumulation of High Lead Concentration by Exopolymer and Whole Cells of Lead-Resistant Bacterium *Acinetobacter junii* L. Pb1 Isolated From Coal Mine Dump." *Environmental Science and Pollution Research* 24: 10652–10661.

Luong, J. H. T., E. Majid, and K. B. Male. 2007. "Analytical Tools for Monitoring Arsenic in the Environment." *Open Analytical Chemistry Journal* 1: 7–14.

Malasarn, D., C. W. Saltikov, K. M. Campbell, J. M. Santini, J. G. Hering, and D. K. Newman. 2004. "arrA Is a Reliable Marker for As(V) Respiration." *Science* 306: 455.

Nigam, S., P. S. Vankar, and K. Gopal. 2013. "Biosorption of Arsenic From Aqueous Solution Using Dye Waste." *Environmental Science and Pollution Research* 20: 1161–1172.

Ordóñez, E., M. Letek, N. Valbuena, J. A. Gil, and L. M. Mateos. 2005. "Analysis of Genes Involved in Arsenic Resistance in *Corynebacterium glutamicum* ATCC 13032." *Applied and Environmental Microbiology* 71, no. 10: 6206–6215. https://doi.org/10.1128/AEM.71.10.6206-6215.2005.

Ordoñez, O. F., M. C. Rasuk, M. N. Soria, M. Contreras, and M. E. Farías. 2018. "Haloarchaea From the Andean Puna: Biological Role in the Energy Metabolism of Arsenic." *Microbial Ecology* 76: 695–705.

Qin, J., B. P. Rosen, Y. Zhang, G. Wang, S. Franke, and C. Rensing. 2006. "Arsenic Detoxification and Evolution of Trimethylarsine Gas by a Microbial Arsenite S-Adenosylmethionine Methyltransferase." *Proceedings of the National Academy of Sciences of the United States of America* 103: 2075–2080.

Sher, S., S. Z. Hussain, and A. Rehman. 2020. "Multiple Resistance Mechanisms in *Staphylococcus* sp. Strain AS6 Under Arsenite Stress and Its Potential Use in Amelioration of Wastewater." *Journal of King Saud University* 32, no. 7: 3052–3058. https://doi.org/10.1016/j.jksus.2020.08.012.

Simeonova, D. D., D. Lièvremont, F. Lagarde, D. A. E. Muller, V. I. Groudeva, and M.-C. Lett. 2004. "Microplate Screening Assay for the Detection of Arsenite-Oxidizing and Arsenate-Reducing Bacteria." *FEMS Microbiology Letters* 237: 249–253.

Singh, A., R. Tiwari, A. Sharma, et al. 2016. "Taxonomic and Functional Diversity of the Culturable Microbiomes of Epigeic Earthworms and Their Prospects in Agriculture." *Journal of Basic Microbiology* 56: 1009–1020.

Smith, E., I. Kempson, A. L. Juhasz, J. Weber, W. M. Skinner, and M. Gräfe. 2009. "Chemosphere Localization and Speciation of Arsenic and Trace Elements in Rice Tissues." *Chemosphere* 76: 529–535.

Suhadolnik, M. L. S., A. P. C. Salgado, L. L. S. Scholte, et al. 2017. "Novel Arsenic-Transforming Bacteria and the Diversity of Their Arsenic-Related Genes and Enzymes Arising From Arsenic-Polluted Freshwater Sediment." *Scientific Reports* 7, no. 1: 1–17. https://doi.org/10.1038/s41598-017-11548-8.

Sun, Y., E. A. Polishchuk, U. Radoja, and W. R. Cullen. 2004. "Identification and Quantification of arsC Genes in Environmental Samples by Using Real-Time PCR." *Journal of Microbiological Methods* 58: 335–349.

Tsuchiya, T., A. Ehara, Y. Kasahara, N. Hamamura, and S. Amachi. 2019. "Expression of Genes and Proteins Involved in Arsenic Respiration and Resistance in Dissimilatory Arsenate-Reducing *Geobacter* sp. Strain OR-1." *Applied and Environmental Microbiology* 85, no. 14: e00763-19. https://doi.org/10.1128/AEM.00763-19.

Uppal, H., H. Hemlata, J. Tawale, and N. Singh. 2016. "Zinc Peroxide Functionalized Synthetic Graphite: An Economical and Efficient Adsorbent for Adsorption of Arsenic (III) and (V)." *Journal of Environmental Chemical Engineering* 4: 2964–2975.

Wolfe-Simon, F., J. S. Blum, T. R. Kulp, G. W. Gordon, S. E. Hoeft, and J. Pett-Ridge. 2011. "A Bacterium That Can Grow by Using Arsenic Instead of Phosphorus." *Science* 332, no. 6034: 1163–1166. https://doi.org/10.1126/science.1197258.

Yamamoto, S., and S. Harayama. 1996. "Phylogenetic Analysis of *Acinetobacter* Strains Based on the Nucleotide Sequences of gyrB Genes and on the Amino Acid Sequences of Their Products." *International Journal of Systematic Bacteriology* 46: 506–511.

Supporting Information

Additional supporting information can be found online in the Supporting Information section.